

Schwarz Domain Decomposition for the Convected Helmholtz Equation: Analysis of Transmission Conditions

Philippe Marchner^[0000-0002-5459-3337]

1 Introduction

We are interested in applying the Schwarz method to the convected Helmholtz equation in unbounded domains, which is of particular interest in aeroacoustics and helioseismology. The equation describes wave propagation in the time-harmonic regime under a general background velocity field $\mathbf{v}(\mathbf{x})$. In this note, we assume a spatially-constant velocity field. Using the $e^{+i\omega t}$ convention, we study the simplified, dimensionless problem

$$\mathcal{L}u = \Delta u - (\mathbf{v} \cdot \nabla)^2 u - 2i\omega(\mathbf{v} \cdot \nabla u) + \omega^2 u, \quad + \text{outgoing radiation condition} \quad (1)$$

under the condition of a subsonic flow $|\mathbf{v}| < 1$, and where the radiation condition is problem-dependent (e.g., one-way, Sommerfeld in free field, or modal basis expansions for waveguides). First, we derive the convergence factor using a Fourier analysis, and explain the role played by the complex advection operator $2i\omega(\mathbf{v} \cdot \nabla)$. Second, we discuss efficient transmission conditions in order to accelerate the convergence of the Schwarz method, and introduce the AAA algorithm for rational approximation of the square-root symbol [11]. Third, we highlight the challenge of applying PMLs as transmission condition, and explain for the first time why a robust PML formulation is compulsory for domain decomposition. This note aims at providing a self-contained analysis with complementary details to studies on OSM for convected propagation, initiated in [7] and further pursued in [6, 9]. The present work focuses on constant velocity fields where Fourier analysis is applicable. Extension to spatially varying velocity fields would require microlocal analysis techniques.

Philippe Marchner
Université Grenoble Alpes, France, e-mail: philippe.marchner@univ-grenoble-alpes.fr

2 Fourier convergence analysis

We consider the two-dimensional unbounded domain $\Omega = \mathbb{R} \times [0, H]$ in the xy -plane, that we split into two subdomains $\Omega_0 = (-\infty, \delta) \times [0, H]$ and $\Omega_1 = (0, +\infty) \times [0, H]$, where δ is the size of the overlap. Following [3], we write the iterative Schwarz method at iteration $(n + 1)$ for the errors $e_i^{(n)} = u_i^{(n)} - u|_{\Omega_i}$, $i = \{0, 1\}$ as

$$\Delta e_0^{(n+1)} - (\mathbf{v} \cdot \nabla)^2 e_0^{(n+1)} - 2i\omega \left(\mathbf{v} \cdot \nabla e_0^{(n+1)} \right) + \omega^2 e_0^{(n+1)} = 0 \text{ in } \Omega_0 \quad (2)$$

$$(1 - v_x^2) \partial_{\mathbf{n}_0} e_0^{(n+1)} + \iota \mathcal{S}_0(e_0^{(n+1)}) = (1 - v_x^2) \partial_{\mathbf{n}_0} e_1^{(n)} + \iota \mathcal{S}_0(e_1^{(n)}) \text{ at } x = \delta, \quad (3)$$

in subdomain Ω_0 , with transmission operator \mathcal{S}_0 and outward normal $\mathbf{n}_0 = (1, 0)^T$. In subdomain Ω_1 we have, with transmission operator \mathcal{S}_1 ,

$$\Delta e_1^{(n+1)} - (\mathbf{v} \cdot \nabla)^2 e_1^{(n+1)} - 2i\omega \left(\mathbf{v} \cdot \nabla e_1^{(n+1)} \right) + \omega^2 e_1^{(n+1)} = 0 \text{ in } \Omega_1 \quad (4)$$

$$(1 - v_x^2) \partial_{\mathbf{n}_1} e_1^{(n+1)} + \iota \mathcal{S}_1(e_1^{(n+1)}) = (1 - v_x^2) \partial_{\mathbf{n}_1} e_0^{(n)} + \iota \mathcal{S}_1(e_0^{(n)}) \text{ at } x = 0, \quad (5)$$

and outward normal $\mathbf{n}_1 = (-1, 0)^T$. Here, \mathcal{S}_0 and \mathcal{S}_1 should approximate the Dirichlet-to-Neumann operators on their respective interfaces to ensure convergence. Homogeneous Neumann conditions are imposed on $y = 0$ and $y = H$ for both problems. Using a Fourier analysis in space $e^{-\iota(k_x x + k_y y)}$, the solution is the sum of incoming (-) and outgoing (+) waves

$$e_0(x, k_y) = a_0(k_y) \exp(-\iota k_x^+(x - \delta)) + b_0(k_y) \exp(-\iota k_x^-(x - \delta)) \text{ in } \Omega_0 \quad (6)$$

$$e_1(x, k_y) = a_1(k_y) \exp(-\iota k_x^+ x) + b_1(k_y) \exp(-\iota k_x^- x) \text{ in } \Omega_1 \quad (7)$$

where the wavenumbers k_x^\pm (outgoing/incoming) are obtained by substituting the Fourier ansatz in (1) with zero right-hand side, leading to

$$(1 - v_x^2) k_x^2 + 2v_x k_x (\omega - v_y k_y) + k_y^2 - (\omega - v_y k_y)^2 = 0.$$

Solving the quadratic equation for k_x gives the dispersion relation

$$k_x^\pm = \frac{-v_x \tilde{\omega} \pm \sigma}{1 - v_x^2}, \quad \tilde{\omega} = \omega + v_y k_y, \quad \sigma = \sqrt{\tilde{\omega}^2 - (1 - v_x^2) k_y^2}, \quad (8)$$

where we fix the square root branch cut on the negative real axis (in line with our time-harmonic convention). We remark that $k_x^+ + k_x^- = -2v_x \tilde{\omega} / (1 - v_x^2)$ and $k_x^+ - k_x^- = 2\sigma / (1 - v_x^2)$, and emphasize that the sign of σ governs the group velocity of the wave (the direction of energy propagation). For example, if $v_x > 0$, we can have positive group velocity $\sigma > 0$ but negative phase velocity $k_x^+ < 0$. To avoid exponentially growing solutions at infinity, we must set $a_0 = 0$, and $b_1 = 0$. By denoting s_0 and s_1 the Fourier representation of respectively \mathcal{S}_0 and \mathcal{S}_1 , the interface conditions (3) and (5) at iteration $(n + 1)$ become

$$\begin{aligned} \left(-i(1-v_x^2)k_x^- + \iota s_0\right) b_0^{(n+1)} &= \left(-i(1-v_x^2)k_x^+ + \iota s_0\right) a_1^{(n)} e^{-\iota k_x^+ \delta} \text{ at } x = \delta, \\ \left(\iota(1-v_x^2)k_x^+ + \iota s_1\right) a_1^{(n+1)} &= \left(\iota(1-v_x^2)k_x^- + \iota s_1\right) b_0^{(n)} e^{\iota k_x^- \delta} \text{ at } x = 0. \end{aligned}$$

Rewriting these two equations as amplitude ratios, and using equation (8), we obtain

$$\frac{b_0^{(n+1)}}{a_1^{(n)}} = \frac{\tilde{\omega}v_x - \sigma + s_0}{\tilde{\omega}v_x + \sigma + s_0} e^{-\iota k_x^+ \delta}, \quad \frac{a_1^{(n+1)}}{b_0^{(n)}} = \frac{-\tilde{\omega}v_x - \sigma + s_1}{-\tilde{\omega}v_x + \sigma + s_1} e^{\iota k_x^- \delta}.$$

After a two-side trace exchange, the convergence factor of the Schwarz method reads

$$\rho = \left| \left(\frac{\tilde{\omega}v_x - \sigma + s_0}{\tilde{\omega}v_x + \sigma + s_0} \right) \left(\frac{-\tilde{\omega}v_x - \sigma + s_1}{-\tilde{\omega}v_x + \sigma + s_1} \right) \right|^{1/2} \left| e^{-\iota \frac{\sigma \delta}{(1-v_x^2)}} \right|.$$

As a consequence of complex advection, we see the footprint of the phase shifts by $\pm v_x \tilde{\omega}$ in the convergence factor. In order to get convergence in two iterations, we would like to take $s_0 = -\tilde{\omega}v_x + \sigma$ and $s_1 = +\tilde{\omega}v_x + \sigma$, or equivalently $s_0 = (1-v_x^2)k_x^+$ and $s_1 = -(1-v_x^2)k_x^-$. One iteration of the Schwarz algorithm is indeed an exchange of the outgoing with the incoming trace. However, when $v_x \neq 0$, we have $k_x^+ \neq -k_x^-$, resulting in an asymmetric trace exchange which may affect the interface data to be transmitted as a source to the neighboring subdomain. To be consistent with the outgoing nature of the original problem, we adopt the symmetric choice $s_0 = s_1 = (1-v_x^2)k_x^+$. In practice, σ yields a non-local operator in space [3], which is impractical for standard PDE discretizations. We therefore approximate it by a polynomial or rational function, denoted $\hat{\sigma}$, to obtain a sparse, local operator representation. Hence, we have $s_0 = s_1 = -v_x \omega + \hat{\sigma}$, yielding

$$\rho = \left| \left(\frac{\hat{\sigma} - \sigma}{\hat{\sigma} + \sigma} \right) \left(\frac{\hat{\sigma} - \sigma - 2v_x \tilde{\omega}}{\hat{\sigma} + \sigma - 2v_x \tilde{\omega}} \right) \right|^{1/2} \left| e^{-\iota \frac{\sigma \delta}{(1-v_x^2)}} \right|. \quad (9)$$

As a counterpart, this choice introduces an asymmetry through the term $-2v_x \tilde{\omega}$, and convergence properties will depend on the sign of v_x . A comprehensive treatment of asymmetric transmission conditions would require further analysis.

3 Performance of transmission conditions

In this section, we show how the choice of $\hat{\sigma}$ impacts the convergence of the Schwarz method. We adopt the notation $s := s_0 = s_1$. We choose $v_y = 0$ to simplify the presentation, but the extension to a general flow direction follows the same principle [9]. Selecting $\hat{\sigma}$ as a second-order polynomial in the Fourier variable k_y incur no extra cost for its operator implementation, while a rational function requires auxiliary fields on the interface [1], increasing the cost per subdomain solve.

3.1 Approximations for propagative modes

We first focus on convergence in the propagative regime, when $\sigma > 0$. We set an overlap $\delta = 0.02$ to damp evanescent modes. The crudest approximation is the Després-like approximation $\hat{\sigma} = \omega$, leading $s = \omega(1 - v_x)$. This choice is optimal for plane waves at normal incidence, since $\sigma \sim \omega$ as $\omega \rightarrow +\infty$, so $\lim_{\omega \rightarrow +\infty} \rho = 0$. The plane wave approximation can be improved using a second-order Taylor expansion

$$\sigma = \omega \sqrt{1 - (1 - v_x^2) \frac{k_y^2}{\omega^2}} = \omega - (1 - v_x^2) \frac{k_y^2}{2\omega} + \mathcal{O}(k_y^4).$$

We plot in Figure 1 the resulting convergence factor for two mean flow directions, $v_x = -0.8$ and $v_x = 0.8$ at $\omega = 30$. We observe a severe deterioration for $v_x > 0$. In particular, there are two peaks in the convergence factor. They can be explained by looking at the denominator of (9). Assuming $\hat{\sigma} \approx \sigma$, the denominator cancels either when $\sigma = 0$ or $\sigma = v_x \omega$. The second condition only exists if $v_x > 0$. Using (8) we obtain two cut-off modes, $k_y = \omega \sqrt{1 - v_x^2}$ and $k_y = \omega$. The frequency range where $v_x > 0$ and $k_y \in [\omega, \omega/\sqrt{1 - v_x^2}]$ is called inverse upstream, because $k_x^+ < 0$ while $\sigma > 0$. In addition, we compute numerically the best second-order approximation of $\hat{\sigma} = a + bk_y^2$, $(a, b) \in \mathbb{C}^2$ by minimizing $\max_{k_y} |\rho(k_y, a, b)|$ over the relevant wavenumber range, following [5]. Note that for $v_x > 0$, we also exclude a small interval around the cut-off mode $k_y = \omega$ to solve the min-max problem. We can

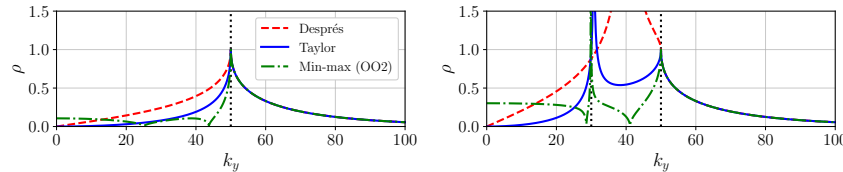


Fig. 1 Convergence factor (9) associated to Després, second-order Taylor and min-max transmission operators for $v_x = -0.8$ (left) and $v_x = 0.8$ (right) at $\omega = 30$, with an overlap $\delta = 0.02$. Black dotted vertical lines show the cut-off modes. OO2: optimized order 2.

design even better approximations of σ by using rational approximations. Figure 2 shows, on a log-scale, the convergence factor for diagonal Padé approximations as $k_y \rightarrow 0$, as well as for near-optimal min-max rational approximations, obtained with the AAA algorithm [11], an adaptive method that constructs barycentric rational interpolants by iteratively selecting optimal support points. While Padé approximations are by design the most accurate for plane waves, min-max approximations show an approximately constant error distribution in the range $k_y \in (0, 50)$, as seen in Figure 2. We next explain how to extend such approximations in the entire spectrum, which is crucial in the non-overlapping case ($\delta = 0$).

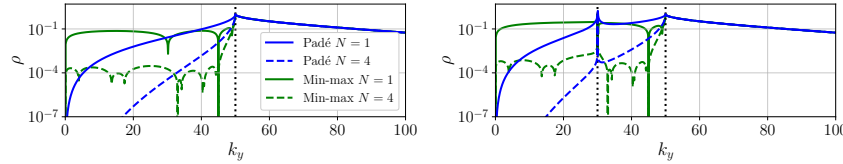


Fig. 2 Convergence factor (9) associated to rational transmission operators of order N for $v_x = -0.8$ (left) and $v_x = 0.8$ (right) at $\omega = 30$, with an overlap $\delta = 0.02$. Black dotted vertical lines show the cut-off modes.

3.2 Extension to the entire spectrum

Designing approximations in the entire spectrum is more challenging, because evanescent modes lie precisely on the branch cut of the square root function $z \mapsto \sqrt{1+z}$. Based on an idea from [10], we redefine the square-root function as $z_\alpha \mapsto e^{i\alpha/2} \sqrt{e^{-i\alpha}(1+z)}$, with $\alpha \in [-\pi, 0]$, moving the branch cut along the ray $R_\alpha = -1 + re^{i(\pi+\alpha)}$, $r > 0$. For example, taking $\alpha = -\pi/2$ moves the branch cut along the imaginary axis. This simple principle allows to extend the validity of the previous approximations to the entire spectrum, which has been exploited in different contexts, see e.g. [1]. Figure 3 shows the obtained second-order Taylor, eight-order Padé and min-max approximations for $v_x = 0.8$. Only well-designed rational approximations are effective in the presence of a strong background flow. Min-max methods are appealing but require re-solving the optimization problem for

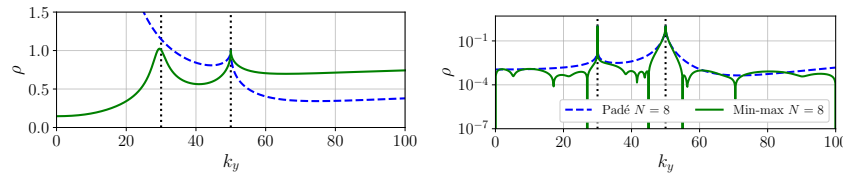


Fig. 3 Convergence factor (9), with $\alpha = -\pi/2$ in the non-overlapping case associated to second-order polynomial (left) and eight-order rational (right) transmission operators for $v_x = 0.8$ at $\omega = 30$. Black dotted vertical lines show the cut-off modes.

each value of v_x . One perspective would be to evaluate the coefficients on the fly by pretraining a neural network on the exterior DtN map [13].

3.3 Perfectly Matched Layers as transmission condition

In the past years, there has been an increasing usage of Perfectly Matched Layers (PML) as transmission condition for optimized Schwarz methods. In their discrete form, PMLs are indeed rational approximations to the exterior DtN map. For con-

vected propagation, it is known that PMLs act on the wavenumber k_x^\pm and not on the group velocity carried by the sign of σ . This may result in a numerical solution that grows exponentially in the PML. We expect a similar behavior for the Schwarz method. However in domain decomposition the interface unknowns encode both incoming and outgoing traces of the error solution (6) and (7). As a consequence, as soon as $v_x \neq 0$, one of the wavenumbers k_x^\pm might not carry the sign of σ , amplifying the error and failing the convergence of the Schwarz method. This is in sharp contrast to using a PML as a radiation boundary condition, where only the outgoing wave needs to be damped, and thus the wavefield decays exponentially when $v_x < 0$. Fortunately, we can follow [2, 8] in order to make the PML act on the sign of σ . In a DDM context, we simply change the PML interface operator by shifting the convection term as $\hat{\mathcal{S}}_{\text{pml}} = -v_x \omega + \mathcal{S}_{\text{pml}}$, and further apply the PML to $\hat{\mathcal{S}}_{\text{pml}}$. This shift prevents the exponential grow of the wavefield in the layer. A strong advantage of the PML lies in its volumetric formulation, allowing selective absorption of the reflected field only, unlike boundary transmission conditions. This enables canceling the incoming wave and act as a source for the outgoing wave.

4 Numerical results on waveguide propagation

We run numerical experiments for a straight waveguide problem oriented along the x -direction, using the GmshDDM [12] solver which is based on finite elements. We use a H^1 -basis composed of integrated Legendre polynomial of order 4, and discretize the problem with 12 points per wavelength. We enforce a multi-modal input boundary condition at $x = 0$, composed by the sum of the first 20 modes with unit amplitude $u_{\text{in}}(0, y) = \sum_{\ell=0}^{19} \cos\left(\frac{\ell\pi}{H}y\right)$, $y \in [0, H]$, satisfying homogeneous Neumann boundary condition at $y = 0$ and $y = H$. The PML formulation from [8] is set as outgoing boundary condition. The waveguide is of unit length and its height is $H = 0.5$. The real part of the solutions at $\omega = 30$, for $v_x = -0.8$ and $v_x = 0.8$, are shown in Figure 4, with $N_{\text{dom}} = 4$ non-overlapping subdomains. We report in Table 1, for different transmission conditions, the number of iterations to reach an interface residual of $r_I = 10^{-6}$ using a Jacobi and GMRES solver. In each case, the relative L^2 -error with the monodomain solution has the same order of magnitude as r_I . We observe that the convergence associated to rational approximation is

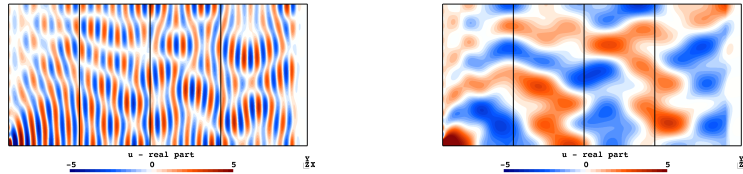


Fig. 4 Real part of the solutions at $\omega = 30$ for $v_x = -0.8$ (left) and $v_x = 0.8$ (right) with $N_{\text{dom}} = 4$. Propagation is along the x -direction. The last subdomain is slightly wider because of the PML.

close to optimal, independently of the mean flow direction, as shown in Table 1 where the number of iterations is close to the number of subdomains. Second-order optimized condition (OO2) perform better than the second-order Taylor condition with $\alpha = -\pi/2$, although we can slightly reduce the number of iterations depending on the scenario by tuning α . For example with $\alpha = -\pi/4$ and $N_{\text{dom}} = 8$, convergence is reached in 51 and 109 iterations, for respectively $v_x = -0.8$ and $v_x = 0.8$. None of the second-order conditions converge for $v_x = 0.8$ with a Jacobi solver. This is because modes 5 and 7 are close to their cut-off frequency (vertical dotted lines in Figs 1, 2, 3), where ρ is large and dominates convergence. GMRES is able to handle the situation. Finally, we illustrate the performance of PML transmission

Table 1 Number of GMRES (Jacobi) iterations to reach $r_I = 10^{-6}$ for $v_x = -0.8$ (left) and $v_x = 0.8$ (right) at $\omega = 30$ for the waveguide problem without overlap. For the Taylor condition we use $\alpha = -\pi/2$. dnc: did not converge. P8: Padé, $N = 8$.

N_{dom}	Despres	Taylor	OO2	P8	N_{dom}	Despres	Taylor	OO2	P8
2	10 (200)	10 (25)	9 (21)	3 (3)	2	17 (dnc)	18 (dnc)	17 (dnc)	3 (3)
4	35 (dnc)	28 (47)	22 (30)	7 (9)	4	57 (dnc)	58 (dnc)	47 (dnc)	9 (9)
8	86 (dnc)	62 (dnc)	46 (dnc)	13 (21)	8	146 (dnc)	133 (dnc)	95 (dnc)	19 (21)
16	166 (dnc)	112 (dnc)	93 (dnc)	25 (45)	16	>200 (dnc)	>200 (dnc)	165 (dnc)	33 (45)

condition for the same waveguide problem at $\omega = 40$. We use a PML of thickness four times the mesh size at the outgoing boundary, and use $N_{\text{PML}} = \{1, 2, 4\}$ layers for the transmission condition. With the standard PML, the Jacobi solver did not converge even in the case $v_x = -0.8$, whereas the shifted PML version converges in all cases. Figure 5 reports the evolution of the interface residual using GMRES. We observe quasi-optimal convergence when the PML is designed appropriately. To summarize, using PML as transmission condition for domain decomposition must be done very carefully for time-harmonic problems with anisotropy. This has been recently highlighted in [4, Example 8.5], with strong anisotropy only in a subset of the domain. The PML transmission condition fails as it amplifies rather than absorbs the wavefield, causing divergence of the Schwarz method.

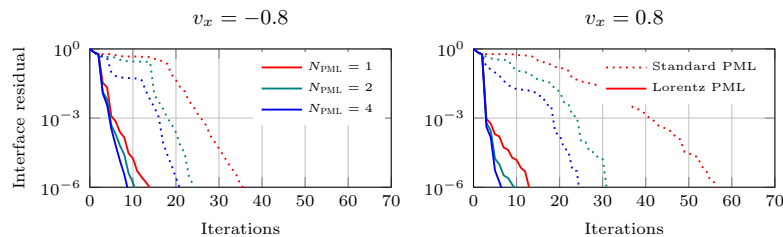


Fig. 5 Residual history for the standard and shifted PML (referred to as Lorentz PML) when used as transmission operators with a GMRES solver, for $N_{\text{dom}} = 4$ and frequency $\omega = 40$.

Acknowledgements I would like to thank Prof. Xavier Antoine, Prof. Christophe Geuzaine, and the two anonymous reviewers for their comments.

References

1. Antoine, X., Darbas, M., Lu, Y.Y.: An improved surface radiation condition for high-frequency acoustic scattering problems. *Comput. Methods Appl. Mech. Eng.* **195**(33–36), 4060–4074 (2006)
2. Bécache, E., Bonnet-Ben Dhia, A.S., Legendre, G.: Perfectly matched layers for the convected Helmholtz equation. *SIAM J. Numer. Anal.* **42**(1), 409–433 (2004)
3. Dolean, V., Jolivet, P., Nataf, F.: An introduction to domain decomposition methods: algorithms, theory, and parallel implementation. *SIAM* (2015)
4. Galkowski, J., Gong, S., Graham, I.G., Lafontaine, D., Spence, E.A.: Convergence of overlapping domain decomposition methods with PML transmission conditions applied to nontrapping Helmholtz problems (2024). ArXiv preprint arXiv:2404.02156
5. Gander, M.J., Magoulès, F., Nataf, F.: Optimized Schwarz methods without overlap for the Helmholtz equation. *SIAM J. Sci. Comput.* **24**(1), 38–60 (2002)
6. Gander, M.J., Tonnoir, A.: Analysis of Schwarz methods for convected Helmholtz-like equations. *SIAM J. Sci. Comput.* **46**(1), A1–A22 (2024)
7. Lieu, A., Marchner, P., Gabard, G., Bériot, H., Antoine, X., Geuzaine, C.: A non-overlapping Schwarz domain decomposition method with high-order finite elements for flow acoustics. *Comput. Methods Appl. Mech. Eng.* **369**, 113223 (2020)
8. Marchner, P., Bériot, H., Antoine, X., Geuzaine, C.: Stable perfectly matched layers with Lorentz transformation for the convected Helmholtz equation. *J. Comput. Phys.* **433**, 110180 (2021)
9. Marchner, P., Bériot, H., Le Bras, S., Antoine, X., Geuzaine, C.: A domain decomposition solver for large scale time-harmonic flow acoustics problems. *SIAM J. Sci. Comput.* **47**(2), B333–B359 (2025)
10. Milinazzo, F.A., Zala, C.A., Brooke, G.H.: Rational square-root approximations for parabolic equation algorithms. *J. Acoust. Soc. Am.* **101**, 760–766 (1997)
11. Nakatsukasa, Y., Setè, O., Trefethen, L.N.: The AAA algorithm for rational approximation. *SIAM J. Sci. Comput.* **40**(3), A1494–A1522 (2018)
12. Royer, A., Béchet, E., Geuzaine, C.: Gmsh-Fem: An efficient finite element library based on Gmsh. In: 14th World Congress on Computational Mechanics (WCCM), ECCOMAS Congress 2020. Scipedia (2021)
13. Taghibakhshi, A., Nytko, N., Zaman, T.U., MacLachlan, S., Olson, L., West, M.: Learning interface conditions in domain decomposition solvers. In: *Advances in Neural Information Processing Systems*, vol. 35, pp. 7222–7235 (2022)